Improvements in transient fidelity of HWIL flight tables using acceleration feedback

Michael Swamp[a] , Colin Stevens[b], Peter Hoffstetter[b]
[a] Acutronic USA Inc, 139 Delta Drive, Pittsburgh, Pennsylvania 15238
[b] Acutronic Schweiz AG, Techcenter Schwarz, 8608 Bubikon, Switzerland

ABSTRACT

Control system architecture will help eliminate or reduce non-linear behavior of flight table axes motions. This elimination and reduction will help improve dynamic transparancy in HWIL simulations. This paper presents the design, analysis and test results of a three-axis hydraulic flight table using acceleartion feedback as a part of the axes servo structure. This approach significantly improves the transient motion of the axis under control producing a very high fidelity flight motion table.

Keywords: Flight Tables Acceleration feedback Motion Fidelity

1. INTRODUCTION

The importance of inner loop feedback to improve the response and robustness of hydraulic servo systems has well been documented. A recent paper, "Improvements in Flight Table Dynamic Transparancy"[1], demonstrates the significant improvement in flight table dynamic performance using a wide band pass, inner loop pressure feedback architecture. The purpose of this paper is not to re-establish this technique, but rather to present the options available for inner loop feedback, and to present the improvements in transient response of hydraulic flight tables that can be achieved with proper feedback sensor selection. We demonstrate the improvements in motion fidelity of using inner loop acceleration feedback for the flight table.

2. FLIGHT TABLE MOTION FIDELITY REQUIREMENTS

Figure 2-1 is a photograph of the Acutronic Model HD7740 three-axis hydraulic flight table shown ready to be inserted into an anechoic chamber for RF seeker simulations.

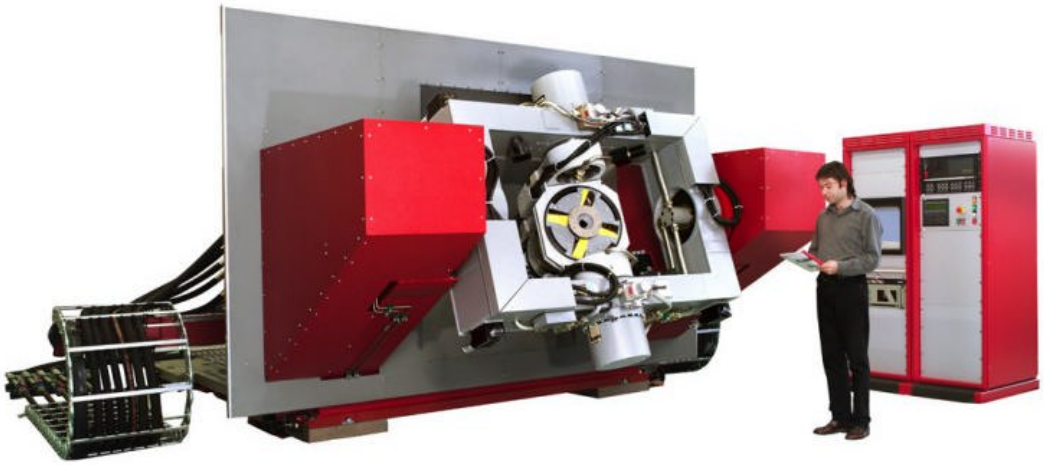

Figure 2-1: Photograph of Acutronic Model HD7740 Three-Axis Hydraulic Flight Table Configured RF Seeker Testing in an Anechoic Chamber

The inner axis of the flight table has a very tight specification on motion fidelity at very low motion dynamics. For a command signal between 1 and 5 Hz with an amplitude of 0.025 degree, the response must exhibit a phase error less than 10 deg and a gain error less than 1 dB from the command. The most common impedement to achieving these very small signal fidelity requirements is the non-linear servo behavior caused by axis friction. This phenomena is exacerbated on the low inertia inner axis. We use low friction actuators on all axes of the flight table; and we typically achieve an axis friction torque less than 0.5% of the axis peak torque. However, on the inner axis we determined that; because the actuator pressure to produce the required accelerations were signficantly lower than the axis friction torque, poor motion fidelity would result. A simple solution to achieve the required motion fidelity on the inner axis is the improvement of the torque disturbance rejection characteristics of the innermost axis servo. We decided to improve the torque disturbance rejection characteristics of the roll axis servo at the inner loop rather than comprise the stability of the position and rate servo paths. We investigated several inner loop servo architectures as candidates for improvement.

3. INNER LOOP CONTROL ARCHITECTURE AND FEEDBACK SENSOR TRADE-OFFS

The servo system engineer has at his disposal a variety of system states to use as inner loop feedback in a hydraulic servo system. In general, the inner loop feedback states to choose from are pressure, torque and acceleration. Figures 3-1, 3-2 and 3-3 are simplified block diagrams showing the servo architecture of pressure, torque and acceleration servo systems respectively including the hydro-mechanical plant and the flexible structure.

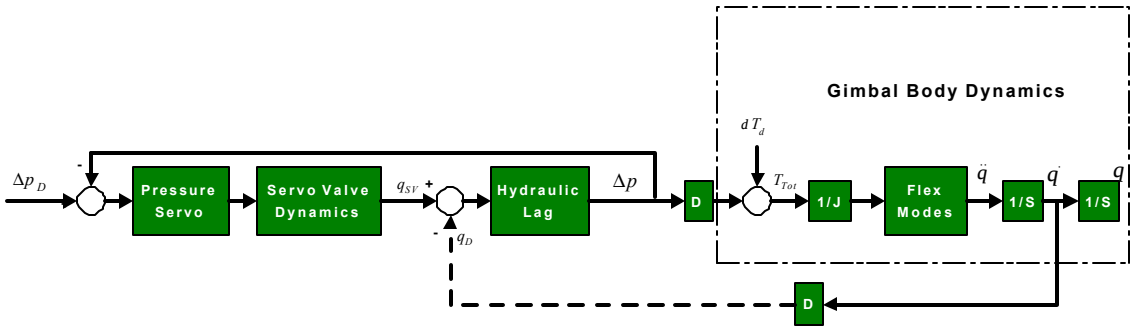

Figure 3-1: Pressure Servo Loop Showing the Hydro -Mechanical Plant with the Flexible Structure and the Mechanical Feedback Path (dashed) Taken from Reference 1

The high pass pressure loop effectively de-couples the hydraulic plant from the mechanical body dynamics and the flexible body modes do not appear in the pressure loop as a dominant structure. Reference 1 describes the benefits of pressure feedback in some detail. While this architecture will significantly improve the dynamic transparency of the overall axis servo; it relies on the rate and position servo loops for torque disturbance rejection.

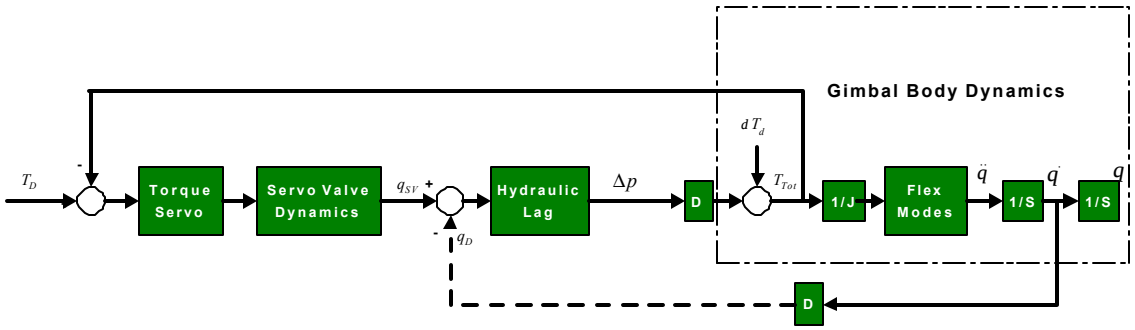

Figure 3-2: Torque Servo Loop Showing the Hydro -Mechanical Plant with the Flexible Structure and the Mechanical Feedback Path (dashed) and Capturing the Torque Disturbance Injection

The high pass torque loop, just as the pressure loop, decouples the hydraulic and mechanical plants with all the resulting benefits. However, the torque feedback architecture provides torque rejection capability without relying on the outer rate and position servo loops.

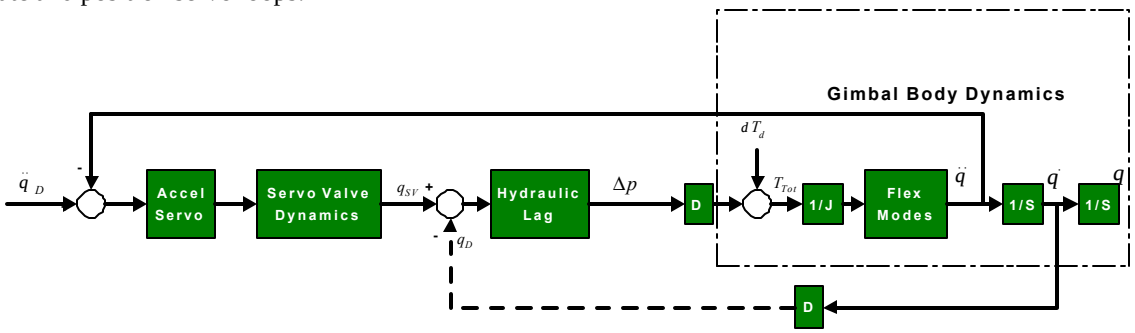

Figure 3-3: Acceleration Servo Loop Showing the Hydro -Mechanical Plant , the Mechanical Feedback Path (dashed) with the Flexible Structure and Torque Disturbance Captured

The acceleration loop, just as in the cases of the pressure and torque loops, decouples the hydraulic and mechanical plants. The acceleration feedback architecture provides torque rejection capability without relying on the outer rate and position servo loops. However the flexible body modes remain within the loop and must be compensated. .

Each feedback state with it's resulting feedback sensor has its specific advantages and disadvantages. Table 3-1 presents a summary of the most common sensors, and the attributes of each.

Table 3-1: Comparison of Inner Loop Feedback Sensors

Feedback State and Sensor	Advantages	Disadvantages
Pressure	• Easily integrated into actuator manifold • Readily available • Typically present on most hydraulic flight tables • Can easily be retrofitted into older systems • Easy to maintain and replace in the field. • Typically the flexible modes of the gimbal are not present in the pressure plant. • Can be calibrated externally from the system.	• Costly. Medium quality sensors and amplifiers can cost over $1500. • One sensor required per actuator, further increasing costs. • Can be easily damaged by pressure spikes, shock isolation required. • Does not, by itself, improve servo torque disturbance rejection capability.
Torque	• Can signficantly improve the servo torque disturbance rejection capability. • Typically the flexible modes of the gimbal are not present in the torque plant. • Sensors are typically robust when installed.	• Costly. Several technologies are available, in most the installation and maintenance cost far outweigh the sensor cost. • One sensor per actuator is required. • Because the sensors need to be mounted to the actuator shaft, the length of the shaft is extended and the overall axis stiffness reduced. • Very difficult to retrofit onto an existing system. • Difficult to replace in the field. • Maintenance of the actuator is more difficult because the sensor must be removed from the actuator shaft for disassembly of the actuator. • Need to be calibrated in place.
Acceleration	• Can signficantly improve the servo torque disturbance rejection capability. • Easily integrated into axis structure • Wide bandwidth, high response sensors are readily available • Very inexpensive, ~$150 / sensor • Can easily be retrofitted into older systems • Easy to maintain and replace in the field • Can be calibrated externally from the system.	• The flexible modes of the gimbals are present and can limit inner loop bandwidth. • Sensors must be used as a pair to eliminate common mode translational acceleration disturbances • Sensor is sensitive to any "on-axis" inertial angular acceleration disturbances .

We immediately eliminated the pressure sensor from consideration because it would not produce the required improvement in the axis torque disturbance rejection. We considered the torque sensor very seriously; but we rejected

it because we could not create enough space on the actuator shaft for placement of the torque sensor. The accelerometer option was deemed the most favorable because (a) it would significantly improve the torque disturbance rejection, (b) the sensors were available off-the-shelf, (c) the inner axis had very high frequency flexible modes that permited a high bandwidth design for the acceleration loop, and (d) the accelerometers could be easily integrated into the axis structure.

4. IMPLEMENTATION

There are a plethora of accelerometer technologies available on the market today. Several characteristics important in the selection of the accelerometer are:

- **Size**. The accelerometer must be compact so it can be easily integrated into the axis stucture.
- **Frequency Response**. The accelerometer must respond to inputs from DC to high frequency.
- **Cross-Coupling**. The accelerometer must be able to reject stimuli in its non-sensitive axes.
- **Noise**. The accelerometer must have a low noise output.
- **Sensitivity**. The accelerometer must produce a usable signal output for the level of acceleration present in the axis.

Of the available sensor types, the peizoresistive sensor was deemed the most suitable. Table 4-1 lists the characteristics of the sensor selected. Figure 4-1 is a picture of the sensor.

Table 4-1: Accelerometer Characteristics

Manufacturer	ICSensors			
Model	3145			
Data sheet	www.msiusa.com/icsensors/catalog/data/accel/M_3145.pdf			
Range	+/- 20G			
Frequency Response	0-500 Hz. Accelerometer resonant frequency over 1 kHz, nearly critically damped.			
	MIN	Typical	MAX	UNITS
Full Scale Output Span	3.6	4	4.2	Volts
Zero Acceleration Output	2.4	2.5	2.6	Volts
Accuracy		0.5	1	+/-% Span
Transverse Sensitivity		1.0	3.0	+/-% Span
Output Noise		0.5		mV p-p

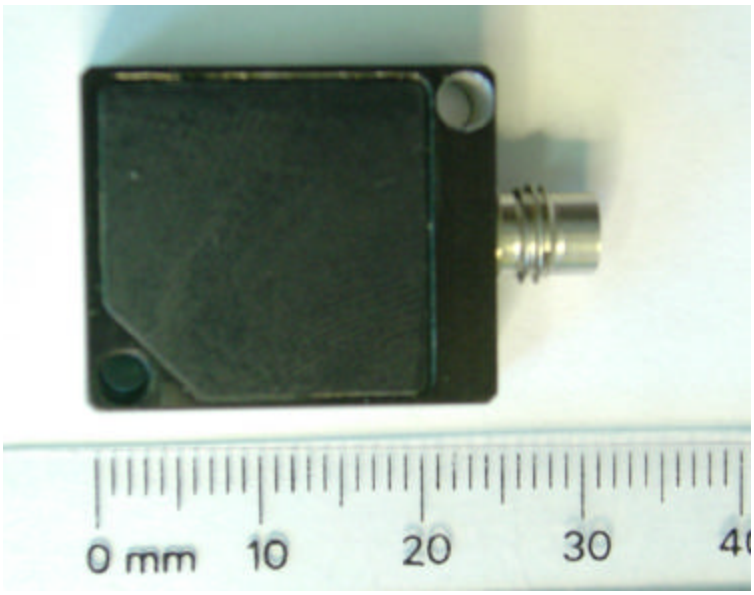

Figure 4-1 - IC Sensors Model 3145

5. COMMON MODE AND ON-AXIS ACCELERATION DISTURBANCES

As mentioned in Table 4-1, in order to obtain usable output from the accelerometers, we must configure the sensors and resulting servo systems to account for common mode and "on-axis" inertial acceleration disturbances. Figure 5-1 shows the general configuration of our three-axis flight table.

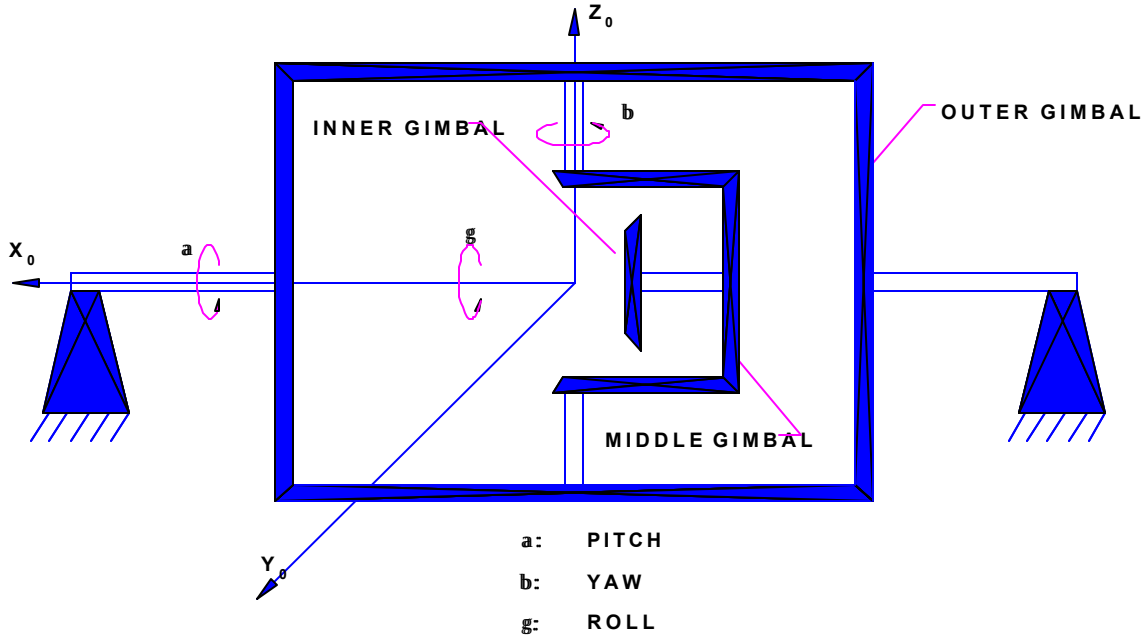

Figure 5-1: General Mechanical Configuration of the Thre e-Axis Flight Table Showing the Inner (Roll), Middle (Yaw) and Outer (Pitch) Axes of Rotation

We install the accelerometers as a pair beneath the inner gimbal tabletop to reject the common mode acceleration. Since the accelerometers are inertial devices they will "measure' the effects of gravity, the centripital force caused by the

angular acceleration, $\ddot{b}$, of the yaw axis and the angular acceleration, $\ddot{a}$, of the pitch axis as the roll and pitch axes line up. The first two effects are common mode disturbances and the last effect is the "on-axis" inertial acceleration disturbances.

Figure 5-2 shows the general mounting arrangement for the sensors on the HD7740 flight motion table roll axis table top. The accelerometers measure the translational acceleration along a fixed radius , R.

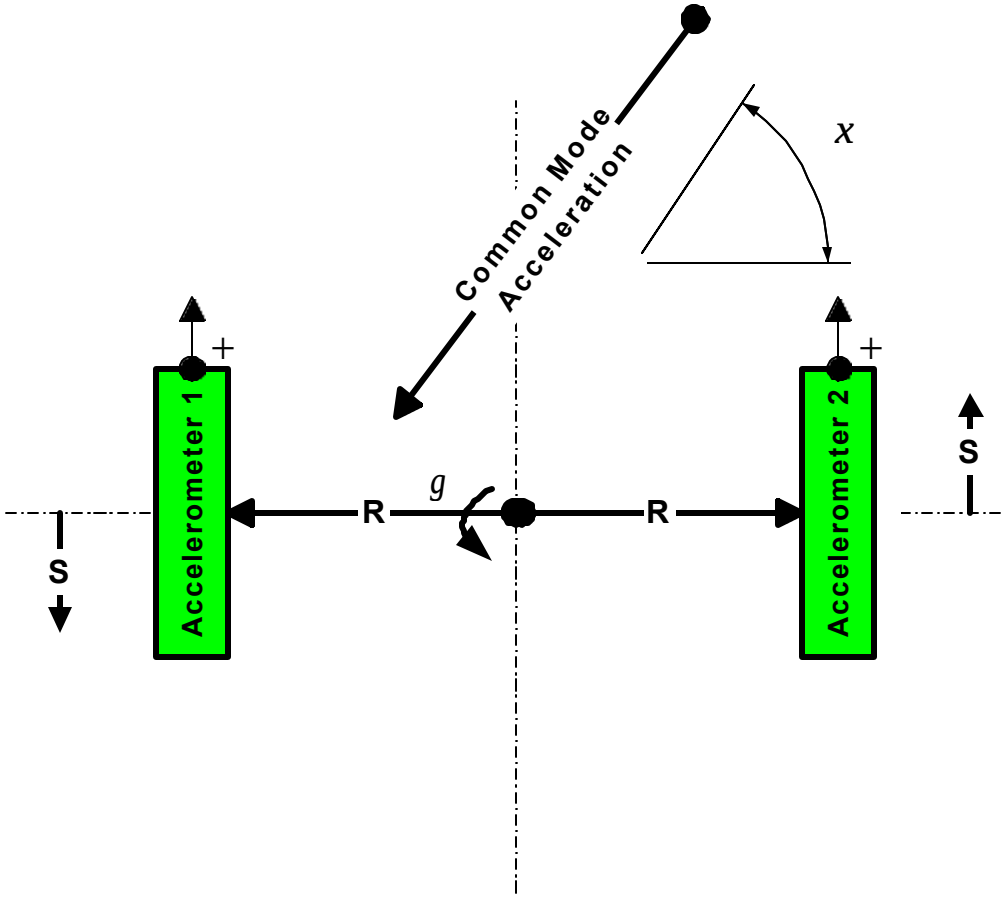

Figure 5-2: Sensor Mounting Arrangement Underneath Tabletop Showing Accelerometer Orientation, Centripital Acceleration, a_c and the Common Mode Disturbance

Figure 5-2 also shows the relationship between the common mode acceleration disturbance and the acceleartion measurements. We want to measure the translational acceleration, $\ddot{S}$; since it is directly proprtional to angular acceleration of the roll axis, $\ddot{g}$,i.e.

$$\ddot{S} = R\ddot{g}$$

In the figure, the measured acceleration seen by the accelerometers will be the sum of the translational acceleration and a portion of the common mode acceleration. The output of accelerometer 1, a_1, will be the negative value of the translational acceleration and the common mode acceleration. The output of accelerometer 2, a_2 , will be the positive value of the translational acceleration and the negative of the common mode acceleration. The measured acceleration may be given as:

$$a_1 = -\ddot{S} - a_{cm}\sin(x) \pm \{\text{Residual}\}$$

$$a_2 = \ddot{S} - a_{cm}\sin(x) \pm \{\text{Residual}\}$$

where a_{cm} is the magnitude of the common mode acceleartion, x is the common mode acceleration angular incidence and $\{\text{Residual}\}$ is the small error due to accelerometer misalignments. By subtracting the two equations we cancel the common mode disturbance and are left with the desired measured output, i.e.

$$\text{Output} = (a_2 - a_1) = 2\ddot{S} \pm \{\text{Residual}\}$$

With proper sensor alignment we can easily ignore the residual and use the desired output as the difference of the two accelerometers.

The on-axis acceleration disturbance on the roll axis consists mainly of the proportion of the pitch axis acceleration cross-coupled to the roll axis due to the angular position of the yaw axis. From Figure 5-1, we can write the angular acceleration disturbance on the roll axis as:

$$d\ddot{g}_d = d\ddot{a}\cos(b) \qquad (5\text{-}1)$$

We can express the pitch axis acceleration disturbance, $d\ddot{a}$, in terms of its Power Spectral Density (PSD), $\Phi_{d\ddot{a}}(w)$, i.e as a band limited white process:

$$\Phi_{d\ddot{a}} = \begin{cases} \dfrac{s^2_{d\ddot{a}}}{w_c}, & 0 \le w < w_c \\ 0 & w_c < w \end{cases} \qquad (5\text{-}2)$$

Where $s^2_{d\ddot{a}}$ and w_c are the variance and cut-off frequency of the band limited pitch axis acceleration disturbance. The RMS value of the of the pitch axis acceleration disturbance, as a function of the pitch axis peak acceleration capability, is:

$$s_{d\ddot{a}} \equiv 0.707\ddot{a}_{Peak} \qquad (5\text{-}3)$$

Finally, the PSD of the roll axis acceleration disturbance is given as:

$$\Phi_{d\ddot{g}} = (\cos(b))^2 \Phi_{d\ddot{a}} \qquad (5\text{-}4)$$

Figure 5-3 shows the roll axis servo system with the acceleration disturbance added.

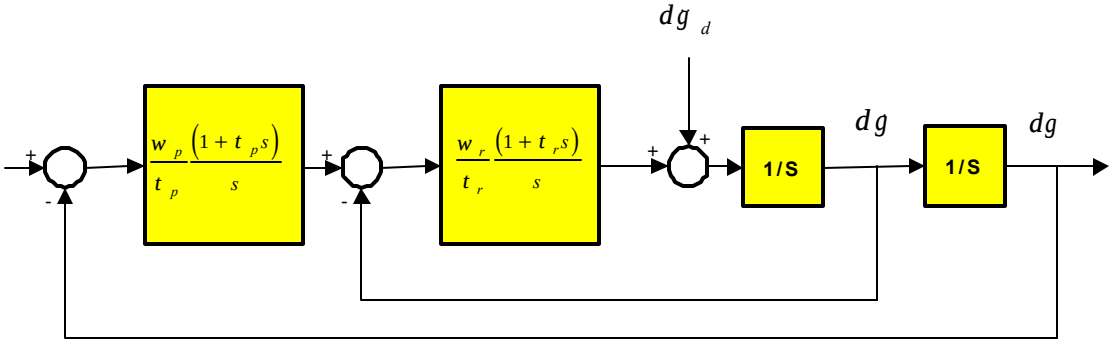

Figure 5-3: Simplified Block Diagram of Roll Axis Servo System, Rate and Position Loops, Showing the "On-Axis" Acceleration Disturbance Injected into the Rate loop

The roll axis servo will reject the on-axis acceleration disturbance within the bandwidth limits of the rate and position loops. We have eliminated the acceleration loop dynamics from the block diagram of Figure 5-3 for simplicity. Although the acceleration loop plays no significant part in the active rejection of the acceleration disturbance, the wide bandwidth performance (~100 Hz) allows the rate and position loop bandwidths to be maximized. From the block diagram of Figure 5-3, the small signal transfer function between the position variation, $dg(jw)$, and the acceleration disturbance variation, $d\ddot{g}_d(jw)$, is:

$$\frac{dg}{d\ddot{g}_d}(jw) = \left(\frac{1}{jw + \frac{w_r(1+jwt_r)}{jwt_r}}\right)\left(\frac{1}{jw + \frac{w_p(1+jwt_p)}{jwt_p}}\right)$$

where w_r and w_p are the rate and position loop crossover frequencies respectively and where t_r and t_p are the rate and position loop lead time constants respectively. For low operating frequency, $w \to 0$, the magnitude of this transfer function reduces to:

$$\left|\frac{dg}{d\ddot{g}_d}_{w\to 0}\right| = \frac{t_r t_p w^2}{w_r w_p}$$

Good servo design practice will set the lead time constants, t_r and t_p to be about two octaves below the loop crossover frequencies, w_r and w_p i.e.

$$t_r = \frac{4}{w_r} \text{ and } t_p = \frac{4}{w_p}.$$

The relationship between roll axis position variation and acceleration disturbance becomes:

$$\left|\frac{dg}{d\ddot{g}_d}_{w\to 0}\right| = \frac{16w^2}{\left(w_r w_p\right)^2} \qquad (5\text{-}5)$$

With this relationship, we can express the PSD of the position variation as:

$$\Phi_{dg} = \left|\frac{dg}{d\ddot{g}_d}_{w\to 0}\right|^2 \Phi_{d\ddot{g}}$$

The variance of the position disturbance as a function of the frequency band of interest (DC to w_0) is given as:

$$s_{dg}^2 = \int_0^{w_0} \Phi_{dg}\, dw = \int_0^{w_0} \left|\frac{dg}{d\ddot{g}_d}_{w\to 0}\right|^2 \Phi_{d\ddot{g}}\, dw$$

From equation 5-5 and 5-2 we have

$$s_{dg}^2 = \int_0^{w_0} \left(\frac{16w^2}{\left(w_r w_p\right)^2}\right)^2 \left(\cos(b)\right)^2 \Phi_{d\ddot{a}}\, dw = \frac{51.2\left(s_{d\ddot{a}} \cos^2(b)\right)^2 w_0^5}{w_c\left(w_r w_p\right)^4} \qquad (5\text{-}6)$$

The RMS value, σ_{dg}, of the position disturbance over selected frequency bands will simply be the square root of the variance from equation 5-5. The peak value of the disturbance can be expressed as:

$$dg = \left(\sqrt{2}\right)\sigma_{dg} \qquad (5\text{-}7)$$

Once we calculate dg from (5-7) we can then calculate the magnitude of the error ratio for the required 0.025 degree amplitude motion. In dB this becomes:

$$\text{error} = 20LOG\left(\frac{0.025+dg}{0.025}\right)\text{dB} \qquad (5\text{-}8)$$

Using equations (5-3), (5-6), (5-7) and (5-8) we can determine the effect of the on-axis acceleration disturbance on the roll axis motion fidelity. Table 5-1 presents the error magnitude results with:

$$\omega_r = 2\pi f_r = 2\pi 60 \text{ rad/sec}$$
$$\omega_p = 2\pi f_p = 2\pi 30 \text{ rad/sec}$$
$$\omega_c = 2\pi f_c = 2\pi 80 \text{ rad/sec}$$
$$\omega_0 = 2\pi f_0,\ f_0 = 1,\ 2.5\ ,5 \text{ Hertz}$$
$$\beta = \beta_0 = 60 \text{ degrees}$$
$$\ddot{\alpha} = \ddot{\alpha}_{max} = 12{,}000 \text{ deg/sec}^2$$

Table 5-1: Error Magnitude Due to "On-Axis" Acceleration Disturbance for Roll Axis Position Amplitude of 0.025 Degrees

Frequency f_0 (Hz)	1	2.5	5
Total error Mag Required (dB)	<1	<1	<1
Calculated error Mag Contribution (dB)	0.005	0.05	0.15

The potential fidelity motion errors caused by either common mode acceleration or acceleration coupled "on-axis" have been practically eliminated by proper system and servo designs.

6. RESULTS

Figures 6-1, 6-2, and 6-3 show the actual response of the roll axis without the acceleration inner loop. The high level of distortion is evident. Figures 6-4, 6-5, and 6-6 show the response of the axis with the acceleration loop. Clearly the performance has been signficantly improved, and is now within the requirements presented in Section 2 above.

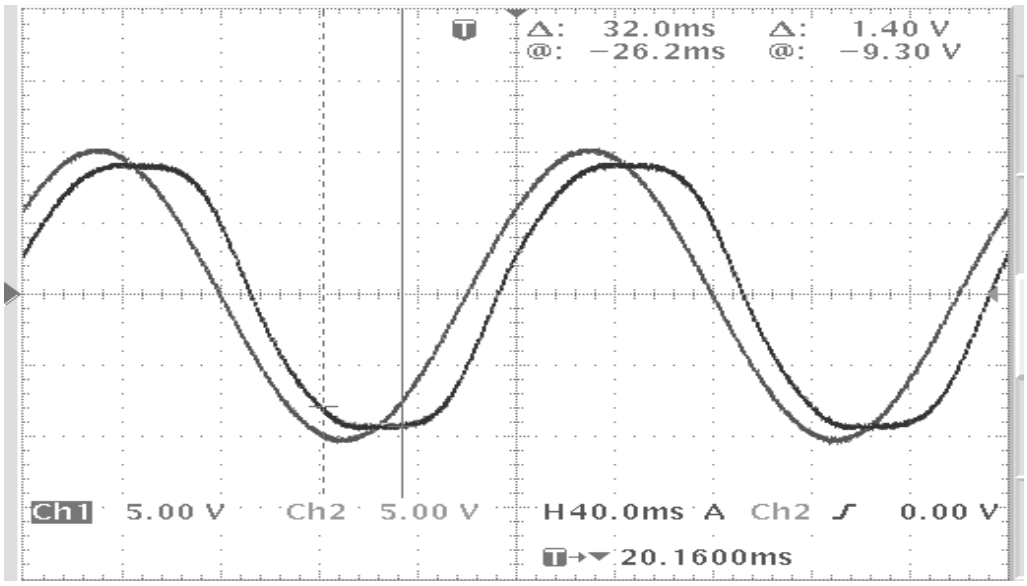

Figure 6-1: Small signal response **without** acceleration loop showing –0.8 dB of gain and 23 deg of phase lag in response to a 5 Hz 0.1 deg pk command

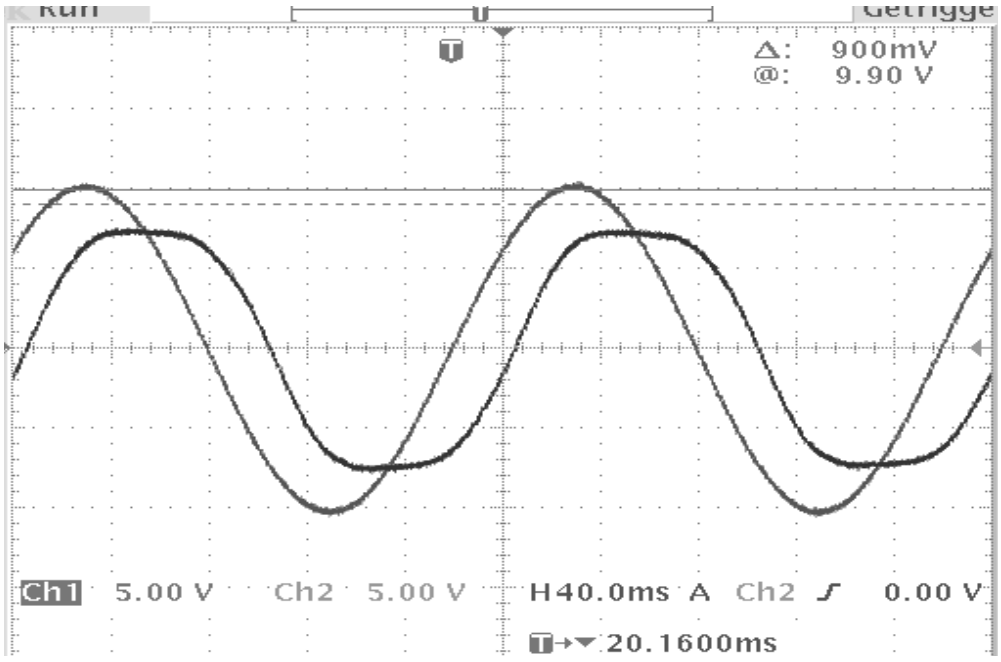

Figure 6-2: Small signal response **without** acceleration loop showing –3.0 dB of gain and 45 deg of phase lag in response to a 5 Hz 0.05 deg pk command

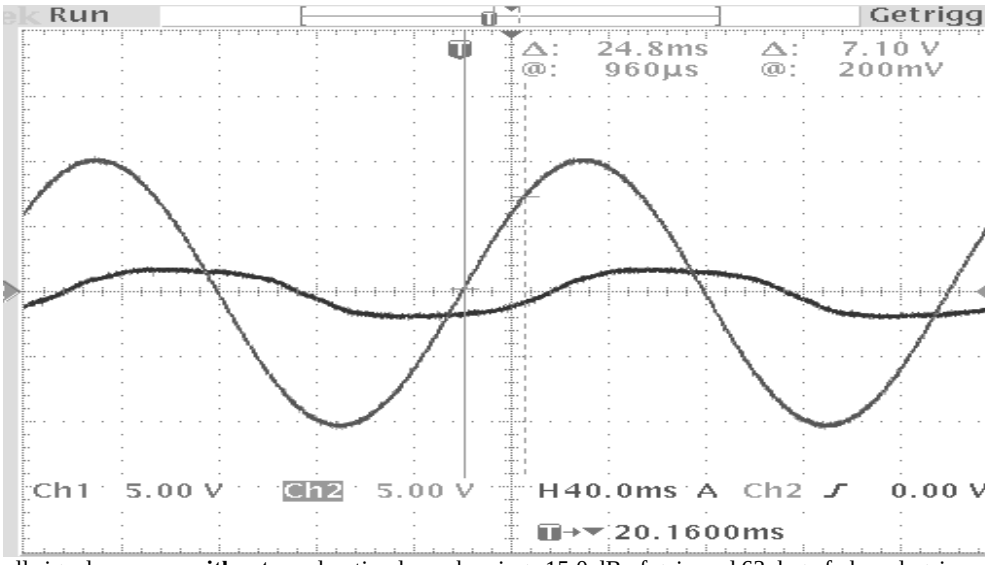

Figure 6-3: Small signal response **without** acceleration loop showing –15.0 dB of gain and 63 deg of phase lag in response to a 5 Hz 0.025 deg pk command

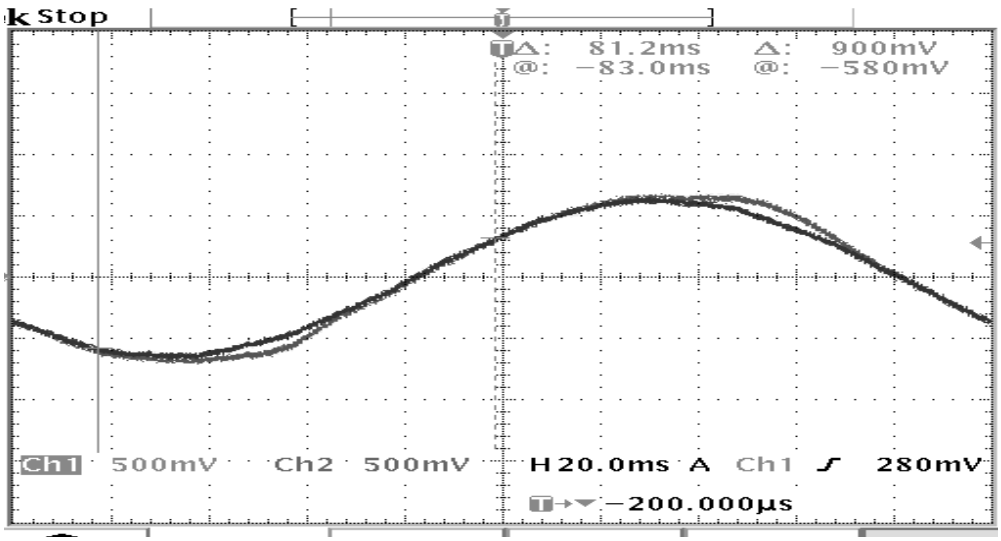

Figure 6-4: Small signal response **with** acceleration loop showing response to a 5 Hz 0.025 deg pk command with a Response Error of ~0.5 dB of gain and ~10 deg of phase lag

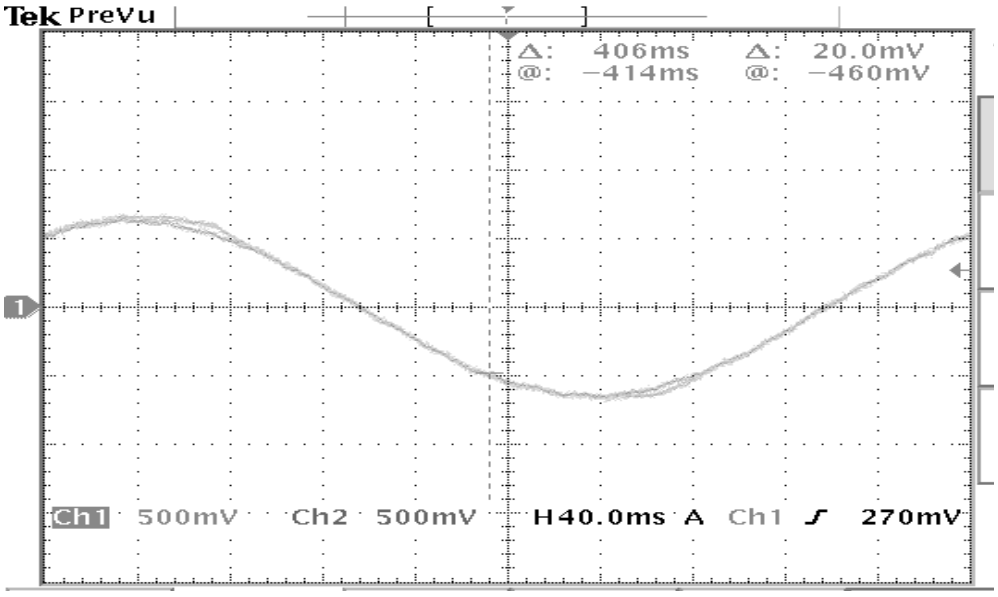

Figure 6-5: Small signal response **with** acceleration loop showing response to a 2.5 Hz 0.025 deg pk command with a Response Error of ~0.1 dB of gain and ~5 deg of phase lag

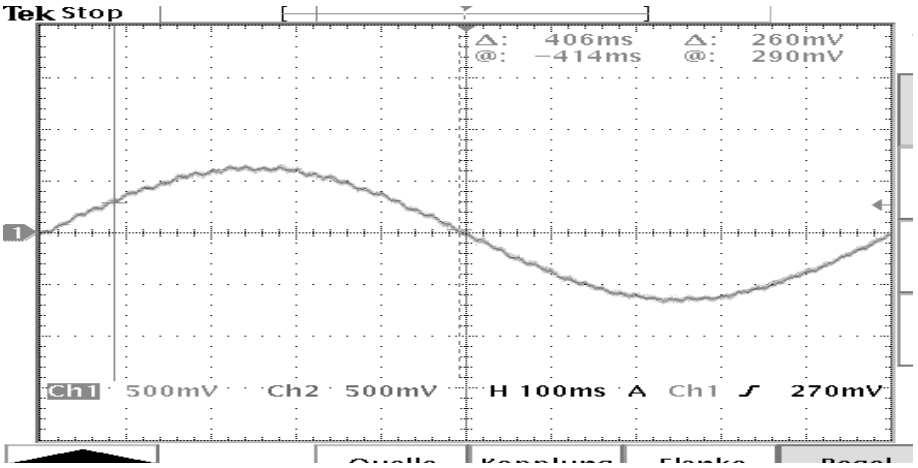

Figure 6-6: Small signal response **with** acceleration loop showing response to a 1 Hz 0.025 deg pk command with a Response Error of 0.05 dB of gain and ~2 deg o f phase lag

Table 6-1 summarizes the results of the motion fidelity testing.

Table 6-1: Motion Fidelity Error Comparison of the Original (without Acceleration feedback) to the Improved (with acceleration feedback)

Command Signal Frequency, Hz	1	2.5	5	5	5
Command Signal Amplitude, (deg)	0.025	0.025	0.025	0.05	0.1
Required Phase Error (deg)	<10	<10	<10		
Original Phase Error, (deg)			-63	-45	-23
Improved Phase error,(deg)	~2	~5	~10		
Required Gain Error, (dB)	<1	<1	<1		
Original Gain Error, (dB)			-15	-3.0	-0.8
Improved Gain Error,(dB)	~0.05	~0.1	~0.5		

The figures and the table clearly demonstrate that the roll axis servo with the acceleration feedback has significantly improved the motion fidelity of the axis. For the phase error, we see improvements of a factor of 6 over the original servo architecture. Similarily, for the gain error, we see improvements of a factor of 30 over the original servo architecture.

7. SUMMARY

Many types of inner loop feedback sensors are available to the servo engineer. Each sensor has its own unique properties, and no single sensor is optimum for every application. Clearly the data presented in this paper demonstrates the importance of proper feedback selection, and the improvements in transient response possible with proper feedback sensor selection.

8. REFERENCES

1. Louis A. DeMore , Paul Mackin, Michael Swamp, Roger Rusterholtz, “Improvements in Flight Table Dynamic Transparency for Hardware-in-the-Loop Facilities”, Proceeding of SPIE Vol.4027 (2000), presented at Aerosense 2000, 24-26 April 2000